Linking Anthropogenic Chlorine Emissions to Regional Air Quality in India

Ankit Patel[1,2*], Malasani Chakradhar Reddy[1,2], Bingqing Zhang[3], Basudev Swain[4], Govindan Pandithurai[1], Meinrat O. Andreae[5,6], Scot T. Martin[7,8], Pengfei Liu[3], Sachin S. Gunthe[1,2*]

[1]Centre for Atmospheric and Climate Sciences, Indian Institute of Technology Madras, Chennai-600 036, India.
[2]Environmental Engineering Division, Department of Civil Engineering, Indian Institute of Technology Madras, Chennai-600 036, India.
[3]School of Earth and Atmospheric Sciences, Georgia Institute of Technology, Atlanta, Georgia 30332, United States.
[4]Atmospheric, Oceanic and Planetary Physics, University of Oxford, Oxford, United Kingdom.
[5] Max Planck Institute for Chemistry, Mainz 55128, Germany.
[6]Scripps Institution of Oceanography , University of California, San Diego, La Jolla, California 92093, United States.
[7]Department of Earth and Planetary Sciences, Harvard University, Cambridge, Massachusetts 02138, United States.
[8]John A. Paulson School of Engineering and Applied Sciences, Harvard University, Cambridge, Massachusetts 02138, United States.

*Corresponding author(s). E-mail(s): ankitpatel0698@cacs.iitm.ac.in; s.gunthe@iitm.ac.in;

Supplementary Material

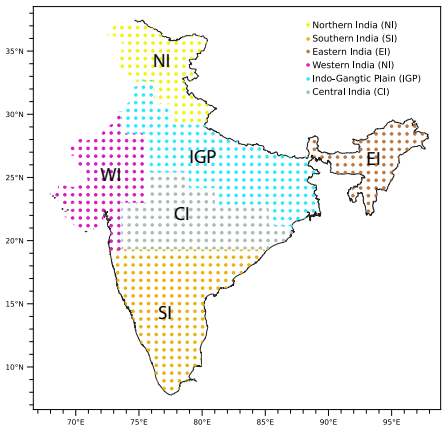

Fig. S1 Indian region divided into six different regions based on different geographical and topographical features [1].

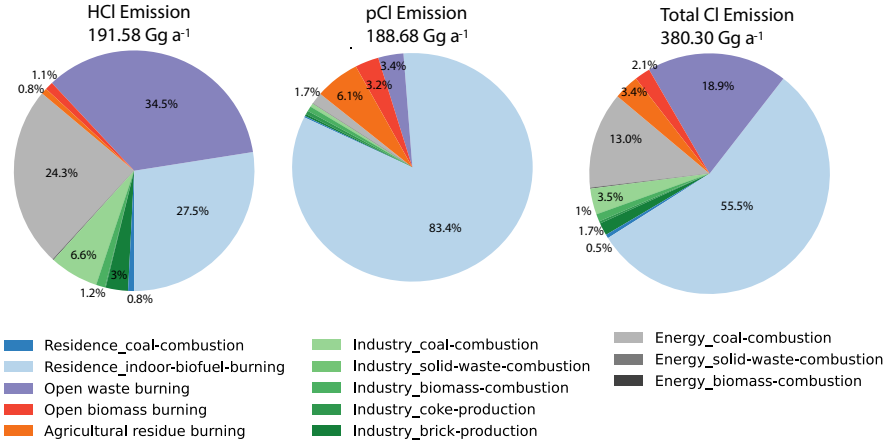

Fig. S2 Pie charts show percentage distribution of HCl, pCl^-, and Total Cl (HCl + pCl^-) annual emissions by source sectors.

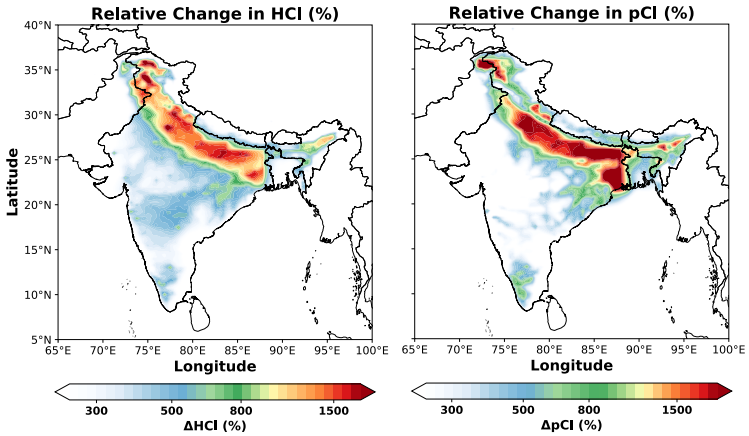

Fig. S3 Annual mean relative changes (%) in HCl and pCl^- concentrations due to anthropogenic chlorine emissions, calculated as the difference between the Wi-AnthroHCl and Wo-AnthroHCl simulations over India.

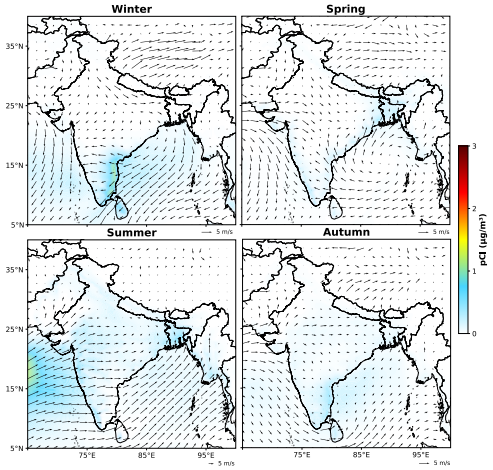

Fig. S4 Seasonal distribution of modelled pCl^- concentrations ($\mu g\,m^{-3}$) from the Wo-AnthroHCl simulation, shown along with wind patterns. The results highlight the strong influence of marine transport on coastal regions across all seasons and the presence of background pCl^- levels even in the absence of anthropogenic chlorine emissions.

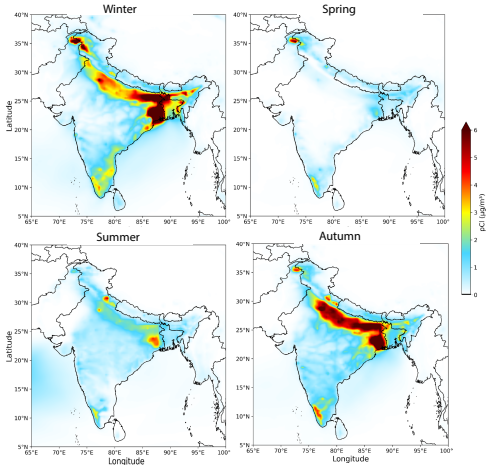

Fig. S5 Seasonal distribution of modelled pCl^- concentrations ($\mu g\,m^{-3}$) from the Wi-AnthroHCl simulation.

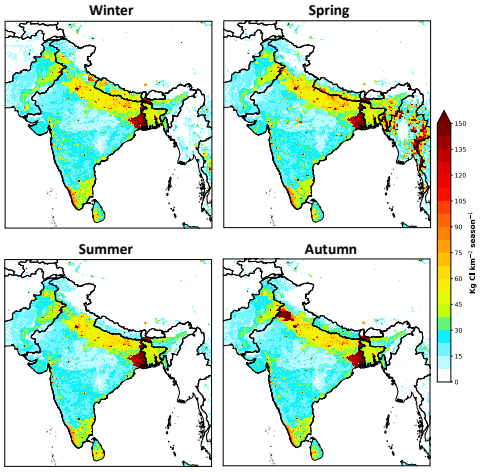

Fig. S6 Seasonal variation of anthropogenic chlorine emissions (HCl + pCl^-) over the study region taken from GT-emission inventory.

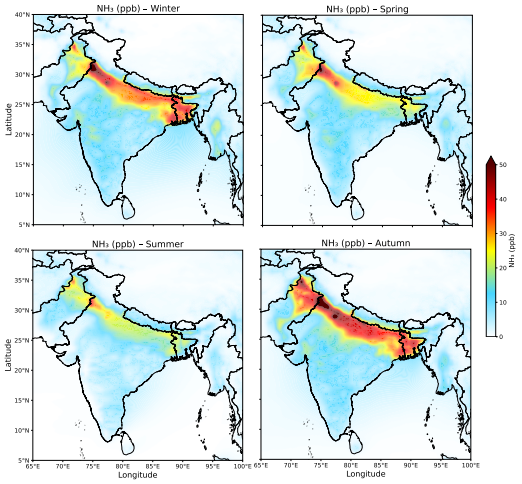

Fig. S7 Seasonal spatial distribution of NH_3 (ppb) from the Wi-AnthroHCl simulation over the Indian subcontinent.

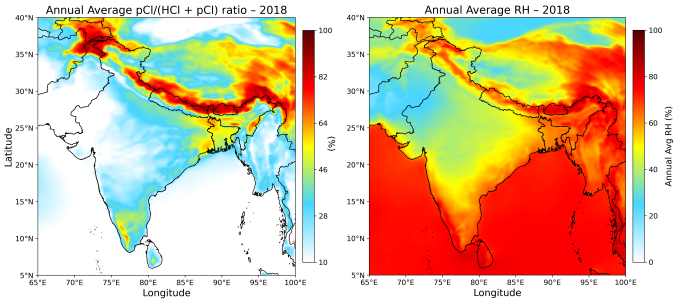

Fig. S8 Spatial distribution of Annual average relative humidity (%) and the pCl^- partitioning ratio efficiency ($pCl^-/HCl+pCl^-$) for 2018.

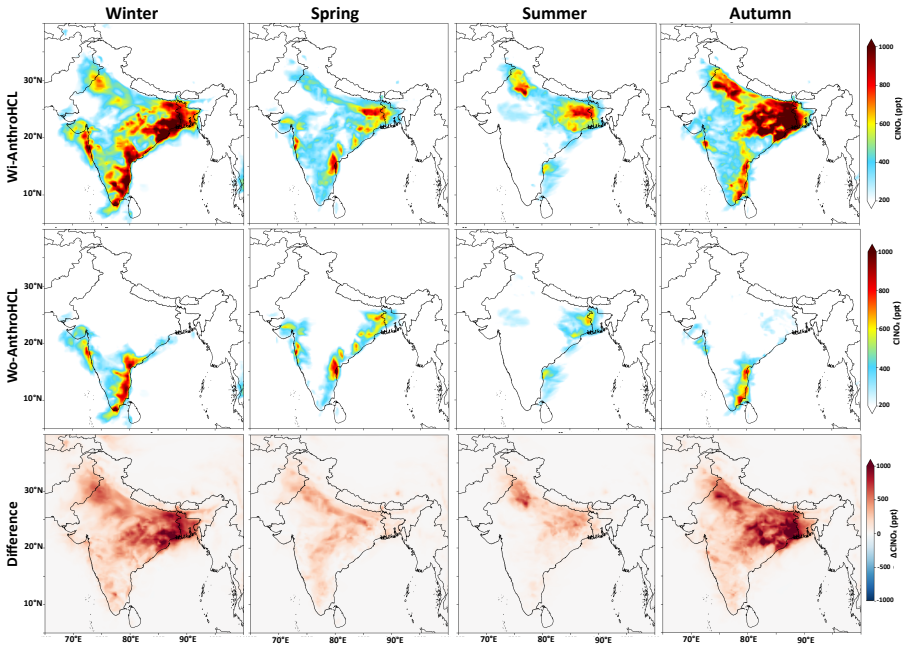

Fig. S9 Spatial distribution of $ClNO_2$ from Wi-AnthroHCl and Wo-AnthroHCl for each season along with the absolute difference between both type of simulation.

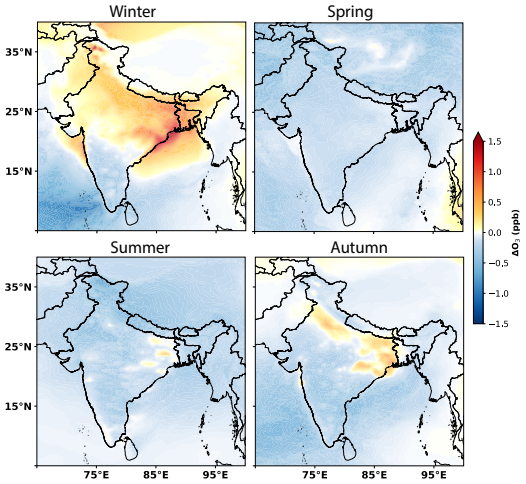

Fig. S10 Spatial distribution of ΔMDA8 O_3 for each season of 2018.

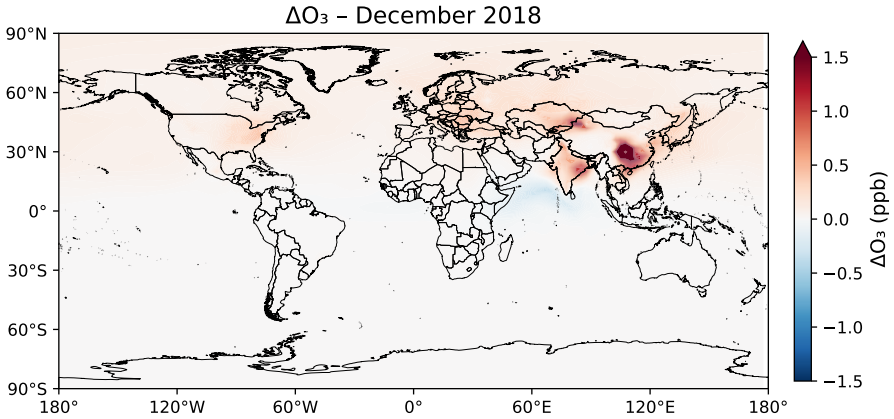

Fig. S11 Global distribution of ΔO_3 for December (2018), calculated as the difference between Wi-AnthroHCl and Wo-AnthroHCl simulations. Despite India being one of the largest contributors to anthropogenic chlorine emissions globally, second only to China, the magnitude of tropospheric ΔO_3 over India is comparatively smaller, indicating a relatively weaker sensitivity of ozone to anthropogenic chlorine emissions in this region.

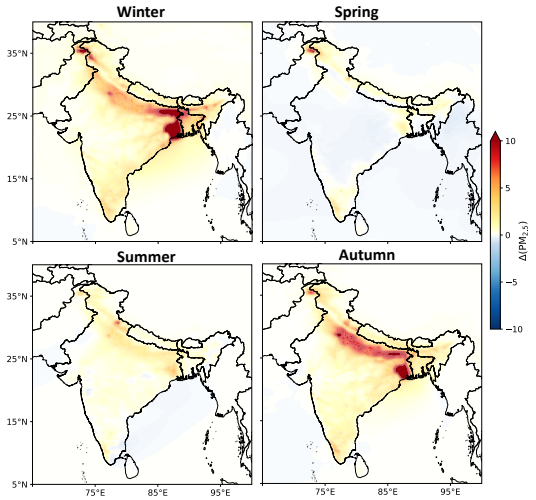

Fig. S12 Spatial distribution of $\Delta PM_{2.5}$ for each season calculated as the difference between Wi-AnthroHCl and Wo-AnthroHCl simulation

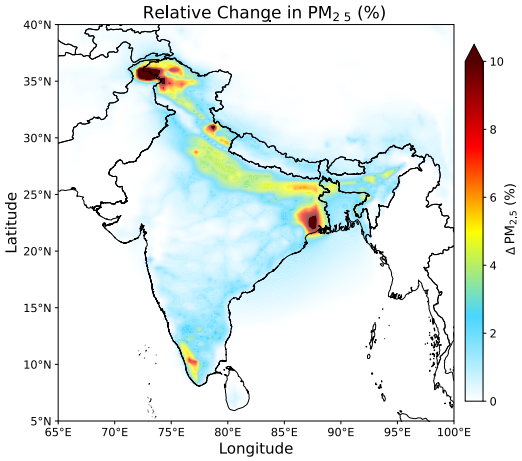

Fig. S13 Annual relative changes (%) in surface $PM_{2.5}$ concentrations due to anthropogenic chlorine emissions, calculated as the difference between the Wi-AnthroHCl and Wo-AnthroHCl simulations over India.

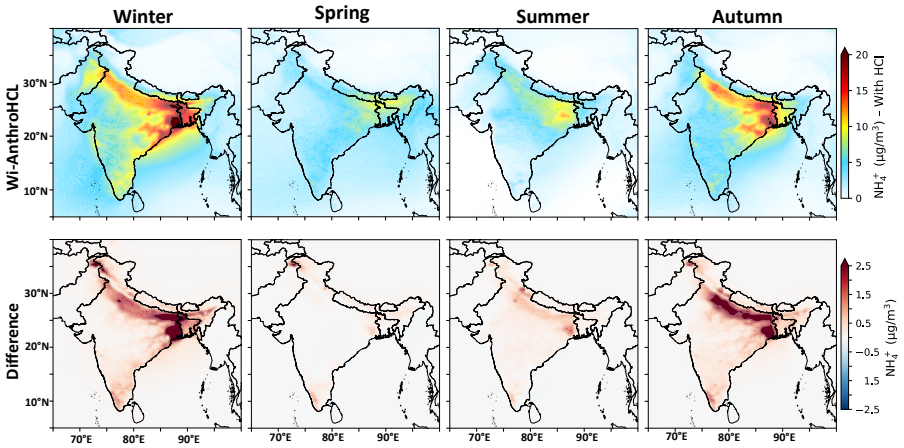

Fig. S14 Spatial distribution of NH_4^+ from Wi-AnthroHCl simulation and the absolute difference between Wi-AnthroHCl and Wo-AnthroHCl simulations for each season.

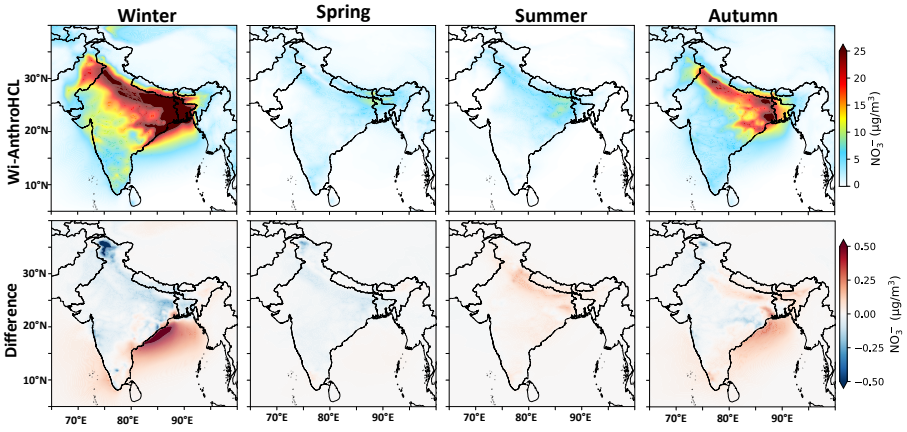

Fig. S15 Spatial distribution of NO_3^- from Wi-AnthroHCl simulation and the absolute difference between Wi-AnthroHCl and Wo-AnthroHCl simulations for each season.

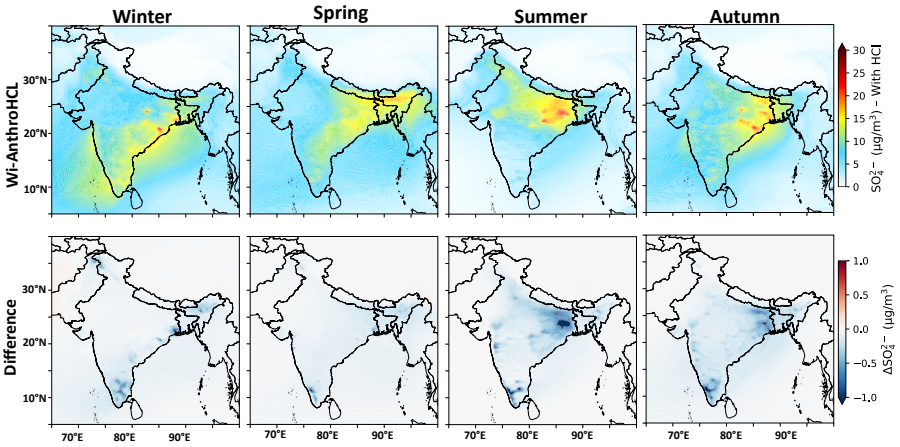

Fig. S16 Spatial distribution of SO_4^{2-} from Wi-AnthroHCl simulation and the absolute difference between Wi-AnthroHCl and Wo-AnthroHCl simulations for each season.

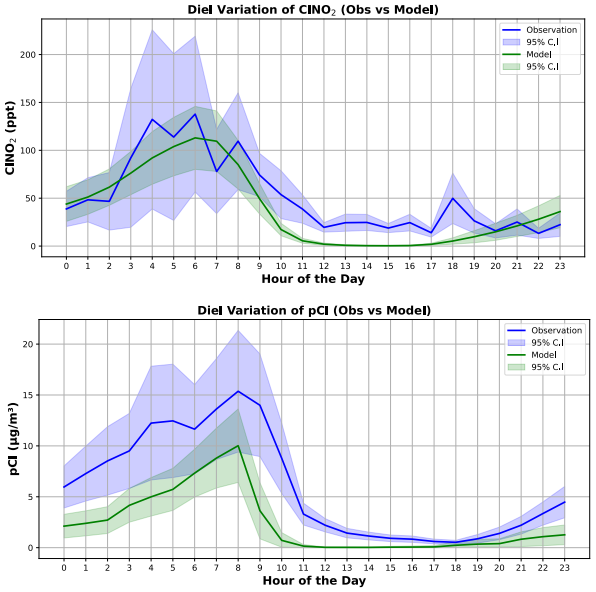

Fig. S17 Model vs Observation of diel variation of $ClNO_2$ and pCl^- at New Delhi, India. Observation data of $ClNO_2$ is taken for January-February 2019 [2] and pCl^- is for February-March from [3].

Table S1 Campaign details of different locations for the pCl^- and $ClNO_2$ observations

Location	Species	Campaign Period	Reference
Ahmedabad (23.03° N, 72.58° E)	pCl^-	September-October 2017	[4]
Kanpur (26.45° N, 80.35° E)	pCl^-	January 2016	[5]
Delhi (28.61° N, 77.23° E)	pCl^-, $ClNO_2$	February-March 2018, January-February 2019	[2, 3]
Chennai (13.08° N, 80.27° E)	pCl^-	January-February 2019	[3]
Mahabaleshwar (17.92° N, 73.65° E)	pCl^-	January-February 2018	This Study
Munnar (10.09° N, 77.06° E)	pCl^-	June-July 2021	This Study

Table S2 Model performance evaluation across campaign sites for pCl^- observations.

Station	Obs Mean	Model Mean	MB	NMB	IOA
Ahmedabad	0.25	0.51	0.26	1.02	0.18
Chennai	0.83	0.54	-0.36	-0.40	0.37
Delhi	5.91	2.68	-3.27	-0.54	0.76
Kanpur	17.65	8.93	-8.72	-0.49	0.62
Munnar	0.18	0.25	0.07	0.41	0.52
Mahabaleshwar	0.09	0.14	0.05	0.56	0.22

Table S3 Model performance evaluation for $PM_{2.5}$ and O_3 in Wi-AnthroHCl and Wo-AnthroHCl model simulations.

	Station	Mean			NMB		r		IOA	
		Obs	Wi-HCl	Wo-HCl	Wi-HCl	Wo-HCl	Wi-HCl	Wo-HCl	Wi-HCl	Wo-HCl
$PM_{2.5}$	Ahmedabad	66.56	63.96	63.32	-0.04	-0.05	0.28	0.29	0.57	0.57
	Chennai	59.04	53.51	52.49	-0.09	-0.11	0.70	0.70	0.81	0.81
	Delhi	82.16	133.66	126.91	0.63	0.54	0.57	0.56	0.62	0.64
	Kanpur	89.24	93.78	89.85	0.05	0.01	0.66	0.65	0.77	0.74
O_3	Ahmedabad	33.88	36.22	36.42	0.07	0.07	0.50	0.48	0.62	0.62
	Chennai	24.96	38.30	38.67	0.53	0.55	0.62	0.62	0.60	0.60
	Delhi	36.66	32.54	32.53	-0.11	-0.11	0.21	0.22	0.50	0.50
	Kanpur	24.97	55.28	55.38	1.21	1.22	0.57	0.57	0.36	0.36

Without pCl^- : Yield: 2 HNO_3 per N_2O_5

$$N_2O_5 + H_2O \longrightarrow 2\,HNO_3 \quad (1)$$

With pCl^- : Yield: 1 HNO_3 per N_2O_5

$$N_2O_5 + pCl^- + H^+ \longrightarrow ClNO_2 + HNO_3 \quad (2)$$

Without HCl emissions: More NH_3 goes to $SO_4{}^{2-}$ formation:

$$2\,NH_3(g) + H_2SO_4(g) \longrightarrow (NH_4)_2SO_4 \quad (3)$$

With HCl emissions: HCl competes for available NH_3 to form NH_4Cl and limits $SO_4{}^{2-}$ neutralization:

$$NH_3(g) + HCl(g) \longrightarrow NH_4Cl \quad (4)$$

References

[1] Malasani, C.R., Swain, B., Patel, A., Pulipatti, Y., Anchan, N.L., Sharma, A., Vountas, M., Liu, P., Gunthe, S.S.: Modeling of mercury deposition in India: evaluating emission inventories and anthropogenic impacts. Environmental Science: Processes &; Impacts (2024) https://doi.org/10.1039/d4em00324a

[2] Haslett, S.L., Bell, D.M., Kumar, V., Slowik, J.G., Wang, D.S., Mishra, S., Rastogi, N., Singh, A., Ganguly, D., Thornton, J., *et al.*: Nighttime NO emissions strongly suppress chlorine and nitrate radical formation during the winter in Delhi. Atmospheric Chemistry and Physics **23**(16), 9023–9036 (2023)

[3] Gunthe, S.S., Liu, P., Panda, U., Raj, S.S., Sharma, A., Darbyshire, E., Reyes-Villegas, E., Allan, J., Chen, Y., Wang, X., *et al.*: Enhanced aerosol particle growth sustained by high continental chlorine emission in India. Nature Geoscience **14**(2), 77–84 (2021)

[4] Singh, A., Satish, R.V., Rastogi, N.: Characteristics and sources of fine organic aerosol over a big semi-arid urban city of western India using HR-ToF-AMS. Atmospheric Environment **208**, 103–112 (2019)

[5] Thamban, N.M., Joshi, B., Tripathi, S., Sueper, D., Canagaratna, M.R., Moosakutty, S.P., Satish, R., Rastogi, N.: Evolution of aerosol size and composition in the Indo-Gangetic Plain: size-resolved analysis of high-resolution aerosol mass spectra. ACS Earth and Space Chemistry **3**(5), 823–832 (2019)